

Targeted nanomedicine with anti-EGFR scFv for siRNA delivery into triple negative breast cancer cells

Phuoc Vinh Nguyen¹; Katel Hervé-Aubert¹; Stéphanie David¹; Nolwenn Lautram²; Catherine Passirani²; Igor Chourpa¹; Nicolas Aubrey³; Emilie Allard-Vannier¹

¹ EA6295 Nanomédicaments et Nanosondes, Université de Tours, Tours, France

² INSERM U1066 / CNRS 6021, équipe MINT, Université d'Angers, Angers, France

³ ISP UMR1282, INRA, équipe BioMAP, Université de Tours, Tours, France

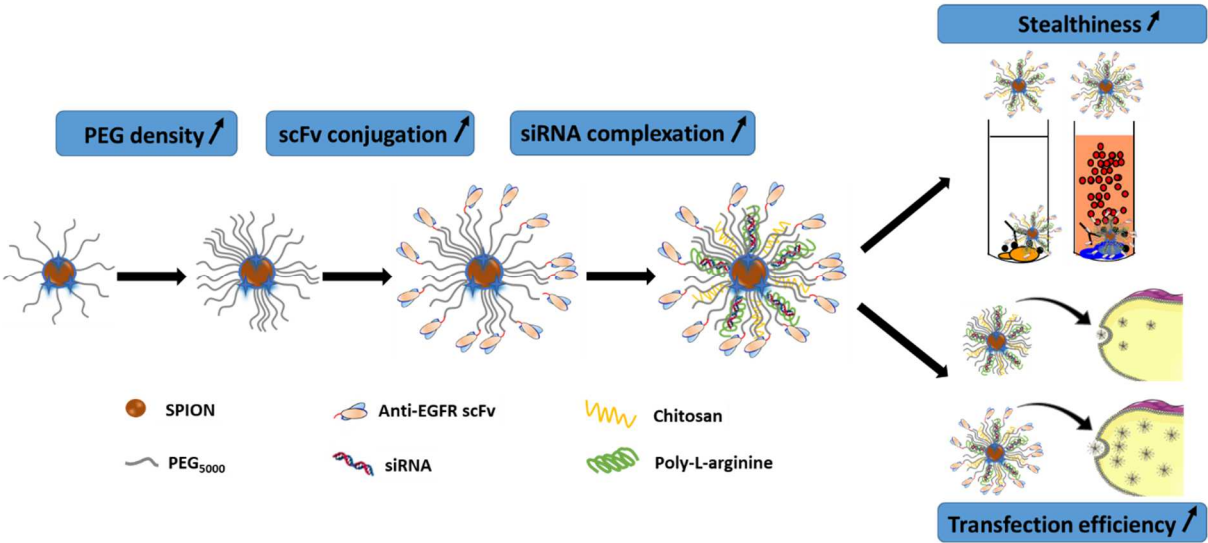
Abstract

A targeted nanomedicine with humanized anti-EGFR scFv (NM-scFv) was developed for siRNA delivery into triple negative breast cancer (TNBC) cells. NM-scFv consisted of i) targeted nanovector (NV-scFv): nano-cargo with targeting properties; ii) siRNA: pharmacological agent and iii) cationic polymers (chitosan, poly-L-arginine): for siRNA complexation and endosomal escape. NV-scFv was based on superparamagnetic nanoparticle (SPION) labeled with DylightTM680, a PEG layer and a humanized anti-EGFR scFv. The PEG density was optimized from 236±3 to 873±4 PEGs/NV-scFv and the number of targeting ligands per NV-scFv was increased from 9 to 13. This increase presented a double benefit: i) enhanced cellular internalization by a factor of 2.0 for a 24h incubation time and ii) few complement protein consumption reflecting a greater stealthiness (26.9 vs 45.3% of protein consumption at 150µg of iron/mL of NHS). A design of experiments was performed to optimize the charge ratios of chitosan/siRNA (CS) and PLR/siRNA (CR) that influenced significantly: i) siRNA protection and ii) gene silencing effect. With optimal ratios (CS=10 and CR=10), anti-GFP siRNA was completely complexed and the transfection efficiency of NM-scFv was 69.4% vs 25.3% for non-targeted NM. These results demonstrated the promising application of our NM-scFv for the targeted siRNA delivery into TNBC cells.

Keywords: TNBC, humanized scFv, gene delivery, targeted nanovector, cationic polymer, active targeting

Abbreviations:

TNBC: triple negative breast cancer; siRNA: small interfering RNA; PEG: polyethylene glycol; NV-scFv: targeted nanovector; NM-scFv: targeted nanomedicine; SPION: superparamagnetic iron oxide nanoparticle; PLR: poly-L-arginine; MS: mass ratio; CS: molar ratio of the positive charges of chitosan amine groups and the negative charges of siRNA's phosphate groups; CR: molar ratio of the positive charges of poly-L-arginine amine groups and the negative charges of siRNA's phosphate groups; EGFR: epidermal growth factor receptor; scFv: single chain variable fragment; NHS: normal human serum.



1 Introduction

Triple negative breast cancer (TNBC) is a complex subtype of breast cancer which is defined by the lack of expression of three receptors: estrogen, progesterone, and human epidermal growth factor 2 (HER2) [1,2]. TNBC is a real challenge for oncologists and considered as the most aggressive subtype of breast cancer due to its highest rate of metastasis, risk of recurrence, and the poorest overall survival [1,3]. Currently, chemotherapy remains the only choice for TNBC systemic treatment but unfortunately, it is limited by poor bioavailability, toxicity, and the emergence of multidrug resistance [3,4]. Therefore, there is an urgent need for new treatment modalities to better manage TNBC.

With more knowledge on the molecular mechanisms of endogenous RNA interference (RNAi), nucleic acid medicines have emerged as innovative modalities for the treatment of incurable diseases such as cancers [5,6]. RNAi's mechanism is based on the interfering activity of double-stranded RNA onto the expression of a particular gene containing a homologous sequence [5]. Three strategies of RNAi including small hairpin RNA (shRNA), micro RNA (miRNA) and small interfering RNA (siRNA) have been largely exploited and are getting more and more interest of worldwide researchers due to its high specificity, significant effect, minor side effects and ease of synthesis [6,7]. Among these strategies, siRNA sequences of 21-23 nucleotides are the most used in the development of anticancer treatment. In fact, most cancers are caused by certain genes encoding for overexpressed proteins, which involve in cancer progress (so-called oncogenes). Rational siRNA sequences can be used to suppress cancer via specific oncogenes' suppression [6,7]. Although the therapeutic potency of siRNA for cancer treatment has been generally accepted, the clinical application of siRNAs remains limited due to extra- and intracellular barriers. Firstly, as the ideal administration route for siRNA is the systemic administration, siRNA is challenged by nuclease activity, kidney clearance, phagocyte uptake, and serum protein's aggregation. Secondly, the highly negative charge and the hydrophilicity of siRNA prevent them from crossing biological membranes. The off-target effect is another challenge for siRNA in *in vivo* applications. This phenomenon refers to the unexpected changes in gene expression sharing partial homology with the siRNA and causes potential toxicity. The last barrier is the recognition of siRNA by the innate immune system that results in the production of inflammatory cytokines. Taking these challenges into account and in order to better exploit the therapeutic potency of siRNA, safe and effective siRNA delivery systems are required [7].

One promising strategy for siRNA delivery is siRNA nanovectorization. This strategy consists in associating siRNA to suitable materials to obtain a nanomedicine (NM) that will be able to i) protect siRNA from nuclease degradation and ii) effectively deliver siRNA to its target. By loading siRNA in nanomedicine, several advantages can be achieved: i) provide serum stability by hiding the charge and the hydrophilicity of siRNA; ii) prolong the blood circulation time by covering the NM with a polymer layer; iii) increase the cellular internalization and intracytoplasmic siRNA release via active targeting and the use of pH-sensitive materials [6]. In this study, siRNA was complexed with cationic polymers surrounding an inorganic core. The presence of the inorganic core was shown to be advantageous for the stability and the size control of the final nanomedicine (NM) [6].

Targeted nanovector (NV) which was based on superparamagnetic iron oxide nanoparticle (SPION) coated with polyethylene glycol (PEG) has been developed in our group as a promising inorganic core for efficient siRNA delivery [2,8]. In addition to its safety in *in vivo* application, siRNA loaded with SPION can combine therapeutic functions and MRI-mediated diagnosis that we call a theranostic approach [8]. Moreover, DylightTM680, a near-infrared fluorescent dye was covalently attached to our SPION core that helped to monitor our nanomedicine in cells and tissues by following its fluorescence signal. Nowadays, the *in vitro* and *in vivo* NM tracking remains a big challenge for NM's commercialization and few studies have focused on this aspect. Thus, this labeling will allow us to overcome this problem. For a successful siRNA delivery system, the stability and stealthiness must be optimized [6]. Therefore, our SPION was covered by PEG₅₀₀₀ shell and one of the main objectives of this study was to optimize the PEG layer's density to obtain the optimal stealthiness. In addition to the passive targeting via the enhanced permeability and retention (EPR) effect, active targeting utilizing biological ligands could provide further advantages such as increased cellular uptake, reduced side effects, and better therapeutic efficacy both *in vitro* and *in vivo* [9].

EGFR overexpression has been observed in almost 70% cases of TNBC and is strictly correlated to tumor proliferation, invasion, and metastasis [16]. Moreover, several studies have been focusing on EGFR targeted nanomedicines for TNBC treatment and have presented preliminary success [10,12,17].

In this study, a specifically designed humanized single chain variable fragment (scFv) directed against epidermal growth factor receptor (EGFR) was chosen as active targeting ligand and conjugated directly on the PEG layer. According to the literature, several ligands have been exploited to target EGFR such as: entire antibodies [10], peptides [11] and aptamers [12].

Compared to the whole monoclonal antibodies (mAbs), this humanized scFv which retains at least one antigen-binding region presents the following advantages: (i) lower molecular weight (25-27kDa vs 150kDa) that keeps our NM small, stable and stealthy; (ii) decreased immunogenicity due to the absence of the Fc constant domain; (iii) possibility to be engineered for a specific conjugation and (iv) ease in synthesis [9,13]. In addition, scFv may overcome the challenge of the peptides' weak binding affinity and the aptamers' degradation by nuclease [14,15].

The targeted nanovector (NV-scFv) was characterized in terms of physicochemical properties and was subsequently associated with siRNA and other cationic polymers to obtain a targeted nanomedicine (NM-scFv) for triple negative breast cancer theragnosis. This inorganic core was necessary for the stability, the size control of the final formulation and the tumor targeting properties. Among the cationic polymers, chitosan and poly-L-arginine (PLR) were chosen for our NM-scFv. These polymers carrying amino groups (NH₃⁺) were complexed with the phosphate groups (PO₄³⁻) of siRNA via electrostatic interactions. This kind of formulation has several advantages such as the ease and rapidity of NM formulation and the prevention from siRNA chemical modification [6]. On the other hand, chitosan is commonly used in siRNA delivery due to its safety, biocompatibility, biodegradability, and its important role in siRNA release into the cytoplasm [2,8]. The second polymer-PLR was added to compensate

the low stability of siRNA-chitosan complex and to increase transfection efficiency at physiological pH [8].

Two siRNA including one control siRNA and one anti-GFP siRNA were used in this study. For further *in vivo* application, siRNA sequences targeting TNBC oncogenes such as anti BCL-xl would be used.

In summary, the targeted nanovector (NV-scFv) with humanized anti-EGFR scFv antibody fragment was firstly developed, physicochemically characterized, and optimized in terms of the PEG layer's density. Secondly, the targeted nanomedicine (NM-scFv) formulation was performed between NV-scFv, siRNA, chitosan, and PLR. The ratios between components were optimized to obtain the maximal siRNA protection and transfection efficiency. Finally, the improvement of our optimized NM-scFv was evaluated concerning the *in vitro* stealthiness and anti-GFP siRNA transfection efficiency.

2 Materials and methods

2.1 Preparation of targeted nanomedicine with anti-EGFR scFv for siRNA delivery

2.1.1 Synthesis of anti-EGFR scFv

The humanized scFv fragment resulted from the association between the heavy (VH) and light (VL) variable domains of an antibody via the (Gly₄Ser)₃ peptide link and the inclusion of peptide flag composed of a hexahistidine tag, a GS spacer and a terminal cysteine at the C-terminus [13]. The design of this humanized scFv fragment was based on the sequences of the variable domains of the chimeric antibody Cetuximab. However, the variable domains have been humanized by removing the N-glycosylation site which is present in the VH and conferring recognition to the protein L for the kappa light chain [18]. So, a gene encoding for humanized scFv was synthesized with an optimized codon for *cricketulus griseus* and cloned in pCDNA3.4 (GeneArt/ Thermo Fisher Scientific). ScFv was produced in ExpiCHO-S™ Cells in a defined, serum-free medium (Thermo Fisher Scientific). ScFv was purified by loading the supernatant onto a HiScreen™ Capto™ L column (GE Healthcare Bio-Science, 17-5478-14). Fractions containing the recombinant proteins were selected at 280nm, pooled, dialyzed against PBS (pH 7.4) overnight, and centrifuged (10,000g, 4°C, 10min). ScFv molecular mass, pI, and molar extinction coefficient data were all generated by the ProtParam tool from <http://web.expasy.org/protparam/>. The fragment was purified in a pure and homogeneous approach according to an analysis on SDS-PAGE (sodium dodecyl sulfate-polyacrylamide gel electrophoresis).

2.1.2 Synthesis of the targeted nanovector (NV-scFv)

The NV-scFv's synthesis was based on the protocol developed by our group [9] and included three steps: (i) the coupling of fluorescent dye onto silanized SPION's surface, (ii) the covering of fluorescent silanized SPION with a PEG layer and (iii) the functionalization of PEGylated SPION with the humanized anti-EGFR scFv. In the fluorescence labelling, 0.5mg of Dylight™680 Amine-Reactive Dye (Thermo Scientific, Rockford, U.S.A) was dissolved in 1mL of anhydrous DMSO and subsequently added into a suspension of 10mL (16mg or 0.287mmol of iron) of silanized SPION

dispersed in DMSO. The suspension was kept under magnetic stirring in dark at room temperature for 24h. NHS-PEG₅₀₀₀-Maleimide (Rapp Polymer, Tuebingen, Germany) was chosen for the polymer layer. NHS-PEG₅₀₀₀-Maleimide was dissolved in anhydrous DMSO and added directly into the fluorescent silanized SPION. The mixture was remained under stirring in dark for 24h. A purification was made by dialysis (MWCO 1000KDa) in the dark against distilled water at 4°C for 48h to eliminate free polymer. Afterward, the conjugation of anti-EGFR scFv (2.1.1) was performed in PBS at pH=7.0 for 24 hours. In order to eliminate all non-conjugated scFv and fluorescent dye, the resulted nanoparticles were purified with size-exclusion chromatography (SEC) using AKTA purifier FPLC system equipped with a prepacked Superdex 200pg column (600x16mm²) (GE Healthcare Bio-Science AB, Uppsala, Sweden) and a PBS 1X solution as the mobile phase (flow rate of 1.6mL/min). The injected volume was 5mL at 0.4g of iron/L and the suspension was detected using a UV/Vis detector at 280nm. At the end of the purification, the NV-scFv was collected and re-concentrated if necessary, with Vivaspin® (cut-off 30kDa, Fisher Scientific, Illkirch, France).

2.1.3 Formulation of the targeted nanomedicine (NM-scFv)

The formulation protocol of NM-scFv was developed and optimized in our group [8,19]. This formulation refers to the siRNA loading onto NV-scFv with the help of two cationic polymers, chitosan (MW=110-150kDa; the degree of acetylation: $\leq 40\text{mol.}\%$, Sigma-Aldrich Chimie GmbH, St. Quentin Fallavier, France) and poly-L-arginine (PLR, MW 15-70kDa, Sigma-Aldrich Chimie GmbH, St. Quentin Fallavier, France). Briefly, control siRNA (Ambion®, New-York, U.S.A) or anti-GFP siRNA (Ambion®, New-York, U.S.A) was precomplexed with PLR while chitosan was mixed with NV-scFv. The complexed siRNA/PLR was then added to the mixture of NV-scFv/chitosan and homogenized using micropipette mixing and vortexing. The final siRNA concentration was fixed at 50nM for transfection experiments, 2000nM for physicochemical characterization, and 190nM for internalization assay. Mass ratio (MS) was used to determine the NV-scFv/siRNA ratio and was fixed at 10. The cationic polymers' content was defined as the charge ratio or the molar ratio of the positive charges of polymers and the negative charges of siRNA. For the optimization of NM-scFv, the charge ratio of chitosan/siRNA (CS) was varied from 10 to 50 and that of PLR/siRNA (CR) from 2 to 10.

2.2 Physicochemical characteristics

2.2.1 Size and zeta potential analysis

The hydrodynamic diameter (D_H), the polydispersity index (PDI), and the zeta potential (ζ) were determined using a Nanosizer apparatus (Zetasizer®, Malvern Instrument, UK). For NV-scFv, the measurement of D_H and ζ was made in PBS 1X or NaCl solution (0.01M) respectively at the concentration of 50mg of iron/L. For the NM-scFv, the measurement was performed after dilution at 1:25 (v/v) of NM-scFv in NaNO₃ 0.01M to fix the ionic strength. The D_H was based on intensity. All the measurements were achieved at 25°C in triplicate and presented in mean values \pm SD.

2.2.2 Determination of NV-scFv and NM-scFv concentration

The concentration of NV-scFv and NM-scFv was expressed in iron concentration (mg of iron/L) or in siRNA concentration (nM). The total iron concentration was determined by atomic absorption spectrophotometry (iCE 3000 spectrometer, Thermo Instruments, France). NV-scFv and NM-scFv were digested by adding concentrated hydrochloric acid (6M) for at least 2h and then diluted with hydrochloric acid (0.12M). Measurements were performed at 248.3nm, and the concentration of the samples was determined using a calibration curve (iron concentrations of 0.25; 0.5; 1.0; 2.0 and 5.0mg/L).

2.2.3 Determination of the polymer layer's density

The grafted polymer density was interpreted via the number of polymer chains per NV. Firstly, the concentration of PEG (mg/L) was quantified using the modified Dragendorff method [20] based on the formation of PEG-Bil₄⁻ complex. The reaction was made between 5mL NV suspension at 10mg of iron/L and Dragendorff's reagent in excess - a solution of potassium bismuth iodide in acetic acid at 3.669M (pH=2.1) for a final volume of 10mL during 15min at room temperature. The absorbance at 520nm of the resulted solution was measured. The NHS-PEG₅₀₀₀-Maleimide concentration of the samples (C_{PEG}) was determined using a calibration curve (NHS-PEG₅₀₀₀-Maleimide concentrations of 0; 12.5; 25.0; 37.5; 50.0; 62.5 and 75mg/L) and the silanized SPION was used as the negative control. The number of polymer chains per NV was then calculated based on the following formula:

$$\text{Concentration of PEG/NV (mole of PEG/g of iron): } C_{PEG/NV} = \frac{2.C_{PEG}}{10.M_{PEG}}$$

$$\text{Number of polymer chains per NV} = C_{PEG/NV} \cdot \frac{\pi D_H^3}{6} \cdot d \cdot 6 \cdot 10^{23}$$

with M_{PEG}= 5311g/mole; d: masse density of SPIONs and determined at 5.2x10⁶g/m³; D_H: hydrodynamic diameter of NV (m), Avogadro's number= 6.10²³mole⁻¹.

2.2.4 Quantification of grafted antibody fragments

The anti-EGFR scFv concentration conjugated onto NV-scFv was determined by a modified Bradford assay [21] using the Coomassie Plus Assay Kit (Thermo Scientific, Rockford, U.S.A) according to manufacturer's instructions. The absorbance of the samples was measured at 630nm and the concentration of scFv (µg/mL) was determined using a calibration curve (scFv concentrations of 0; 2.5; 5; 10; 15; 20; 25µg/mL) and NV without scFv was used as the negative control. This concentration was transferred into mole of scFv per g of iron and the number of scFv/NV was finally calculated using the same formula for the calculation of the number of polymer chains.

2.2.5 Functionality test of grafted antibody fragments

The functionality of the grafted anti-EGFR scFv was evaluated by indirect enzyme-linked immunosorbent assay (ELISA). In this experiment, EGFR recombinant protein (Sino Biologicals, Beijing, P.R. China) was coated in a 96-well plate at 2µg/mL in PBS and incubated overnight at 4°C. The wells were then saturated with 3% of BSA-PBS for 1h at 37°C. Afterward, PBS for the negative

control, NV-scFv, or NV (from 0.003 to 100mg of iron/L) was incubated in wells for 1h at 37°C. The wells were subsequently washed with PBS-Tween 20 (0.05%; m/v) and incubated with 100µL of protein L-peroxidase (Pierce®, Thermo Fisher Scientific) diluted at 1.25µg/mL for 1h at 37°C. An enzymatic reaction was made by the addition of 100µL of 3,3',5,5'-Tétraméthylbenzidine substrate (TMB; Sigma, St Louis, USA) and stopped with 50µL of H₂SO₄ 1M. Finally, the absorbance was measured at 450nm using an absorbance microplate reader (Bio-Tek® instruments, Inc., USA). The presence of scFv was revealed by the well coloration and its content is proportional to the absorbance at 450nm.

2.2.6 siRNA protection with agarose gel electrophoresis

To verify the siRNA protection capacity, the electrophoresis technique on agarose gel was used. An agarose gel at 1% (m/v) was prepared containing 0.01% (v/v) ethidium bromide (EtBr) to visualize free siRNA. NM and NM-scFv were formulated in double for each type of NM or NM-scFv. The first sample was diluted with water and the second was diluted with heparin 10g/L (Sigma-Aldrich Chemie GmbH, Steinheim, Germany) at a dilution factor of 2:1 (v/v) in order to destabilize the formulation and release the formulated siRNA. A loading buffer (Agarose gel loading dye 6X, Fisher, Bioreagents®, Illkirch, France) was added and a final content corresponding to 16pmol of siRNA per well was deposited. The migration of samples on the gel was conducted in a Tris-acetate-EDTA (TAE) 1X buffer (Acros Organics, Geel, Belgium) for 15min at 150V. The visualization of free siRNA was made with UV-imaging using the EvolutionCapt software on a Fusion-Solo.65.WL imager (Vilbert Lourmat, Marne-la-Vallée, France).

2.3 Cell culture experiments

2.3.1 Cell culture

Triple negative breast cancer cells MDA-MB-231 (ECACC, Salisbury, U.K.) and MDA-MB-231 expressing GFP (MDA-MB-231/GFP) (Euromedex, Souffelweyersheim, France) were cultured at 37°C in an atmosphere containing 5% CO₂. The culture medium was made of DMEM supplemented with 10% fetal bovine serum, 1% non-essential amino acid (Hyclone Laboratories, Logan, Utah) and 1% penicillin/streptomycin (Gibco®, Life Technologies, Paisley UK). The cell harvesting was made with trypsin/EDTA (0.05%) (Gibco®, Life Technologies, Paisley UK) at 80% of confluence.

2.3.2 Transfection assay

MDA-MB-231/GFP cells were seeded at 3.10⁴ cells/well in a 12-well plate for 24h before the transfection. The day of transfection, NM-scFv, Oligofectamine™, and Lipofectamine™ (Invitrogen, Thermo Fisher Scientific, Paisley, UK) were prepared with anti-GFP siRNA at a final siRNA concentration of 50nM in respect of the formulation protocol and the manufacture recommendation. Cells were treated with NM-scFv in serum-free Opti-MEM (Gibco®, Life Technologies, Paisley UK) or in complete medium (10% of serum) and maintained for 4h. Afterward, the NM-scFv was removed or maintained in normal growth conditions (the supplementation in serum was made for cells treated with Opti-MEM) for 68h until the analysis. Non-treated cells were used as the negative control. Cells were

removed using trypsin and then analyzed with a flow cytometer (Gallios flow cytometer, Beckman Coulter). Data were analyzed using Flowing Software 2.5.1. The siRNA transfection efficiency (gene silencing effect) was calculated by the percentage of the cells with reduced GFP fluorescence intensity over the analyzed cells using the GFP fluorescence histogram.

2.3.3 Cytotoxicity test

Cell viability was evaluated by MTT assay. MDA-MB-231 cells were seeded at 3×10^4 cells/well in a 12-well plate for 24h. Formulations of siRNA, NV-scFv, and PLR at different charge ratios of PLR/siRNA were prepared and incubated with cells for 72h in normal growth conditions. Non-treated cells or cells treated with H_2O_2 at 20mM were used as the negative and positive control respectively. The culture medium was then replaced by the mixture of 190 μ L of fresh medium and 10 μ L of an aqueous solution of MTT (5g/L) and incubated for 4h at 37°C. The medium/MTT mixture was removed and 200 μ L of DMSO was added in each well. The plate was agitated until the homogeneity and the absorbance was measured at 540nm using KC-junior V1.40 software on a BIOTEK EL800 microplate reader. The number of viable cells was directly proportional to the absorbance value and the percentage of viable cells was calculated according to the followed equation:

$$\frac{As - Apc}{Anc - Apc} \times 100$$

As, Apc and Anc are the absorbance of the sample, the positive control and the negative control.

2.3.4 Internalization assay

The internalization of NV and NM into MDA-MB-231 cells was evaluated by following the Dylight™680 fluorescence with flow cytometry. MDA-MB-231 cells were seeded onto a 12-well plate at 1.5×10^5 cells/well. After 24h, NV-scFv or NM-scFv prepared with control siRNA in Opti-MEM was added to cells at a final concentration of 25mg of iron/L (or 190nM in siRNA for NM) for 4h. After 4h, a cell culture medium of 20% of serum was added at a dilution factor of 1:1 (v/v) for 20h. Non-treated cells were used as the negative control. After incubation time, cells were washed, removed using trypsin, and analyzed by flow cytometry.

2.4 Complement activation test (CH50 test)

Complement consumption was assessed in normal human serum (NHS) (Établissement Français du Sang, Pays de la Loire, Nantes, France) by measuring the residual hemolytic capacity of the complement system after contact with NM-scFv. The final dilution of NHS in the mixture was 1:4 (v/v) in 400 μ L of reactive media. The technique consisted in determining the amount of serum that was able to lyse 50% of a fixed number of sensitized sheep erythrocytes with rabbit anti-sheep erythrocyte antibodies (CH50) [22]. Complement activation was expressed as a function of iron concentration to estimate the impact of the polymer coating for a similar quantity of SPIONs. The *in vivo* iron concentration of interest was in the range of 125-188 μ g/mL of NHS. This range was calculated based on the blood-serum volume per mouse (1,4-1,7mL blood or 0.55-0.83mL serum for a mouse of 20-

25g) and the ferrofluid quantity that would be injected per mouse (125 μ L of NM-scFv at 0.83 μ g/ μ L or 103.75 μ g of iron per mouse).

2.5 Experimental design

A full factorial design 2^2 was created by Minitab®16 (Minitab, Inc.) to determine the effect of charge ratios (CR and CS) on the transfection efficiency of anti-GFP siRNA loaded in NM-scFv. This experimental design composed of two independent parameters and one variable response (dependent variable). The independent parameters including CR and CS were studied at two levels. Besides, three central points were included to get an indication of curvature and an estimation of pure error. The transfection efficiency was evaluated as the dependent variable. Each experiment was performed in triplicate and an overview of the experimental design including the results is shown in Table SI 2. To determine the optimal parameters, the optimization function of Minitab was used.

2.6 Statistics

Values were expressed as mean \pm standard deviation (SD). Fisher's ANOVA test was used to evaluate the effect of charge ratios on the transfection efficiency. The effect of charge ratio on transfection efficiency was considered significant when p-value<0.05 (*). For the internalization assay, Student's t-test was used to compare the results and the difference was considered significant when p-value<0.05.

3 Results and discussion

3.1 Development and optimization of the targeted nanovector (NV-scFv)

The synthesis of our targeted nanovector as shown in Fig. 1, was based on the protocol developed in our group for HER2-positive breast cancer with some adaptations [9,13]. Briefly, the three-step synthesis allowed us to modify the surface of initial silanized SPION according to our purposes. It started with the direct introduction of a near-infrared (NIR) fluorescent dye onto the silanized SPION core via the reaction between NHS groups of the fluorophore and the primary amines on the SPION core. In this study, the fluorophore was Dylight™680 with fluorescence emission in the very near infrared. This property was particularly well adapted for *in vivo* optical analysis due to the high transparency of tissues in this spectral region. For a systemic administration, the colloidal stability at physiological conditions and the stealthiness against the immune system are required [23]. One of the most common strategies is to cover our NV-scFv with a PEG layer that increases: i) the stability thanks to steric hindrance [24] and ii) the circulation time by avoiding the recognition by the mononuclear phagocyte system (MPS) via opsonization process [22]. For this purpose, the bi-functional NHS-PEG₅₀₀₀-Maleimide was chosen. The NHS groups reacted with the primary amines of silanized SPION core and the maleimide groups allowed the subsequent conjugation with active targeting ligands. Furthermore, the PEG layer would protect the fluorophore from the quenching by external interactions. Finally, to achieve the active targeting for TNBC, a humanized recombinant anti-

EGFR scFv of the Cetuximab antibody was conjugated to our NV. This conjugation implied the carbodiimide chemistry by creating disulfide bridges between the C-terminal cysteines introduced into the scFv sequence and the maleimide groups of the polymer layer. Our anti-EGFR scFv had been also rationally designed to facilitate its orientation and was coupled selectively onto the polymeric surface of the NV via a site-specific covalent conjugation.

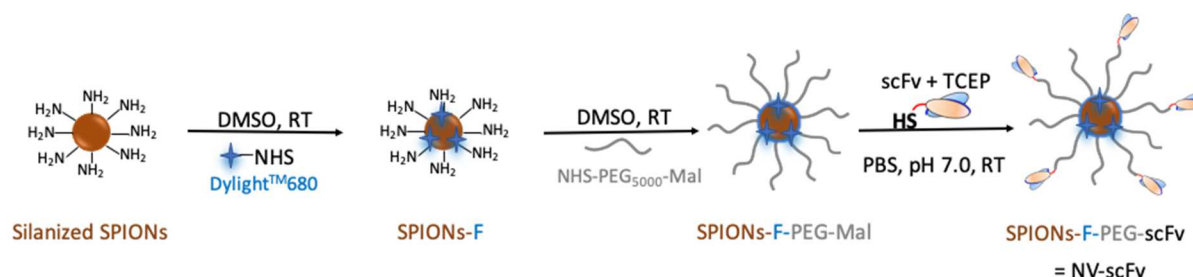


Fig. 1. Schematic representation of targeted nanovector (NV-scFv) synthesis.

3.1.1 Improvement in the polymer density and the number of grafted scFv onto the targeted nanovector

The former results for HER2+ breast cancer showed a perspective of using NV-scFv for tumor active targeting [9]. However, its stealthiness needed to be optimized to achieve a long circulation time allowing a higher *in vivo* tumor accumulation. The developed HER2-targeted NV-scFv was quickly captured and eliminated by the liver and spleen [9]. Facing this problem, we hypothesized that the polymer layer used for HER2 targeted NV-scFv (molar ratio between PEG/iron 0.3) was not sufficient to obtain a relevant stealthiness. The impact of PEGylation on the NV's stealthiness is highly dependent on PEG molecular weight (MW), polymer chain architecture, and surface density of the PEG coating [25]. As the PEG₅₀₀₀ is appropriate in terms of molecular weight [25,26], the enhancement in the density of the PEG layer may be a potential solution [27]. Thus, this research aimed to increase the PEG density by optimizing the ratio of PEG/iron in the synthesis. Three nanovectors were synthesized with different molar ratios of PEG/iron at 0.3 (NV1); 0.6 (NV2); and 0.9 (NV3) respectively using the same initial SPION and the number of polymer chains per NV was determined using the modified Dragendorff method. For the same type of NV (shape) with a similar size, the number of polymer chains per NV was used to evaluate the polymer density [27]. The results showed that by increasing the molar ratio of PEG/iron, an increase in the number of polymer chains per NV was observed between NV2 and NV1: 873 ± 4 PEGs vs 236 ± 3 PEGs/NV respectively. The higher polymer density of NV2 compared to NV1 could consequently improve its stealthiness. Nevertheless, there was no enhancement in the number of polymer chains for NV2 compared to NV3 (873 ± 4 vs 850 ± 10 PEGs/NV). This result suggested a possible saturation in the number of PEGs that can be grafted onto the NV's surface. For this reason, the molar ratio of PEG/iron superior to 0.9 was not further considered.

The increase in the number of polymer chains per NV did not change the physicochemical properties of the nanovector. The size of all evaluated nanovectors was around 80nm with a highly

monodispersed population (PDI inferior to 0.3) and the nanovectors were almost neutral in charge that is required for an injectable form (Table I).

Table I. Number of grafted PEGs, scFv molecules and physicochemical properties of different nanovectors.

	NV1	NV2	NV3	NV1-scFv	NV2-scFv
PEG/iron molar ratio	0.3	0.6	0.9	0.3	0.6
Number of PEG per NV	236±3	873±4	850±10	236±3	873±4
D _H (nm)	76.6±5.3	78.8±0.2	82.8±3.4	78.0± 1.7	74.4 ± 4.0
PDI	0.15±0.01	0.22±0.01	0.10±0.01	0.15±0.02	0.19±0.02
ζ (mV, pH 7.4)	-2.8±2.4	-5.2±1.3	-4.5±1.2	-1.1±1.5	-3.5±1.0
Number of scFv per NV	0	0	0	9	13

Also, the possibility of increasing the polymer density layer led us to a hypothesis: the higher the density of polymer layer is, the more functional groups the nanovector can have on its surface resulting in a higher scFv grafting rate onto the nanovector. To verify this hypothesis, two targeted nanovectors were synthesized from NV1 and NV2 at two corresponding molar ratios of scFv/iron at 1/2000 and 1/1000 respectively. The number of scFv grafted onto NV-scFv was then quantified with a modified Bradford assay. This method exploits the strong red shift of Coomassie G-250 dye (from 465 to 595nm) when it binds to protein and is suitable for SPION-grafted scFv quantification [13]. Consistent with our previous studies, no change in physicochemical characteristics was observed after the conjugation of scFv (Table I). As predicted, more antibody fragments were successfully conjugated onto NV's surface when the polymer density was higher: 13 scFv vs 9 scFv that might improve the targeting properties of our NV.

To verify the functionality of the conjugated scFv, an ELISA assay on increasing concentrations of NV and NV-scFv was carried out with the target protein EGFR and detected by Protein L (PpL). This protein presents a great advantage to detect antibody fragments such as scFv thanks to its ability of binding to some kappa light chain variable domains without interfering with the antigen-binding site [9,18].

As shown in Fig. 2A, while the absorbance of PpL's substrate for the whole range of NV's concentration remained negligible for non-targeted NV, both NV-scFv presented a gradually increasing absorbance. At the same NV's concentration, the absorbance of PpL's substrate for NV2-scFv was higher than NV1-scFv (~0.6 vs ~0.4 at 10mg of iron/L for example). To compare the binding affinity between grafted scFv and free scFv, this experiment was performed also for the same quantity of free scFv as the scFv grafted on NV2-scFv. For the whole studied range of concentrations, there was no difference in the absorbance of PpL's substrate between free scFv and conjugated scFv on NV2-scFv (Fig. 2B).

All the above results indicated i) the possibility to increase the PEG density on NV's surface, ii) the enhancement in PEG density resulted in the increased number of scFv conjugated onto NV-scFv and iii) the preserved functionality of conjugated scFv.

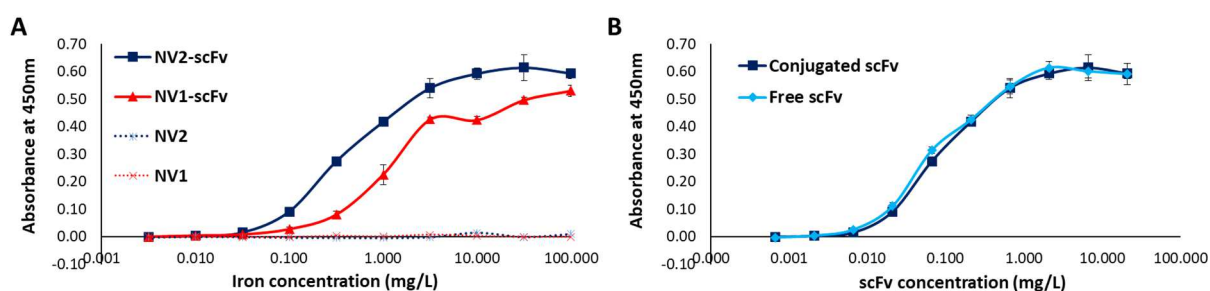


Fig. 2. Functionality interpreted by the absorbance at 450 nm of PpL's substrate obtained from ELISA experiment of conjugated and free anti-EGFR scFv in suspension regarding EGFR protein. A) Conjugated scFv in different NVs and B) Conjugated scFv in NV2-scFv vs free scFv.

3.1.2 Internalization assay into cancer cells of the optimized nanovector

To clarify the benefit of the scFv conjugation onto NV-scFv, cellular internalization of non-targeted or targeted nanovector was performed on MDA-MB-231 TNBC cells. In this experiment, cancer cells were incubated with four types of nanovector including NV1; NV1-scFv; NV2; and NV2-scFv for 24h. The signal of the fluorescent dye of NVs in suspension was checked beforehand and the signal of DylightTM680 was followed using flow cytometry.

As shown in Fig. 3, both functionalized nanovectors with anti-EGFR scFv internalized better into cells than non-targeted NVs by a factor of 2.6 and 4.1 for NV1-scFv vs NV1 and NV2-scFv vs NV2 respectively ($p < 0.01$). This result demonstrated the benefit of active targeting with the humanized anti-EGFR scFv. In addition, the increased number of grafted scFv on the NV2-scFv was shown to be favorable for the cellular internalization. The NV2-scFv internalized better than NV1-scFv by a factor of 2.0 ($p < 0.01$).

These results led us to choose the NV2-scFv for further experiments.

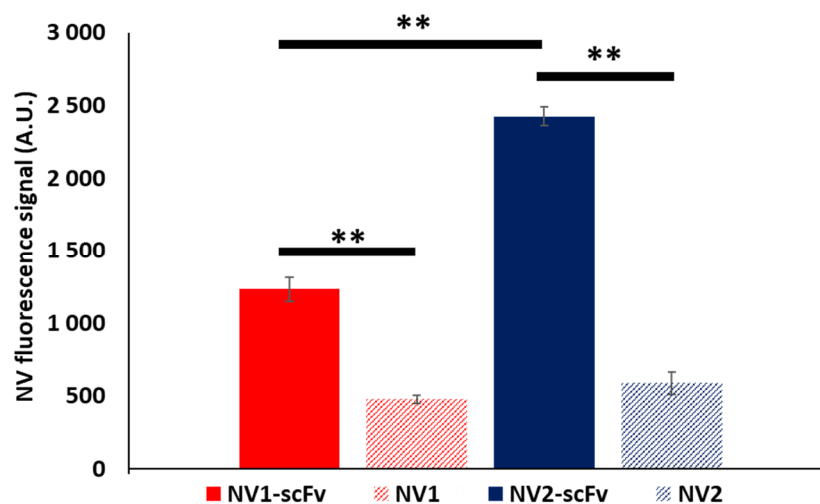


Fig. 3. NV fluorescence signal by following DylightTM680 fluorescence intensity of different NVs internalized into MDA-MB-231 cells. Double asterisk (**) indicates statistically significant factors with $p < 0.01$.

3.2 Optimization of the targeted nanomedicine (NM-scFv) for siRNA delivery

After optimizing the targeted nanovector, the next step was to associate this NV-scFv with siRNA to form the targeted nanomedicine (NM-scFv). Among the available methods, the electrostatic complexation was chosen due to its ease and speed of the preparation [6].

The NM-scFv comprised of three ingredients: i) siRNA to inhibit the expression of targeted oncogenes (in this study, a control siRNA and an anti-GFP siRNA were used as models); ii) NV-scFv which played a key role in the stability, control of the size and targeting properties of the final NM-scFv [6]; and iii) two cationic polymers including chitosan and poly-L-arginine (PLR) which were essential for not only siRNA protection at physiological pH but also an endosomal escape for siRNA transfection efficiency. Concerning the protocol (Fig. 4), the siRNA and NV-scFv were precomplexed with PLR and chitosan respectively. By mixing negatively charged NV-scFv with chitosan, an electrostatic interaction may occur and the chitosan was trapped into the PEG coating. PLR, which produced a more compact complex with siRNA could enable more efficient shielding of the siRNA-PLR charges within the PEG coating of NV. Once siRNA-PLR was added into Chitosan-NV, the siRNA-PLR could trap low-charged chitosan on the NV resulting in a lower size and polydispersity. In cells, with the protonation of chitosan amine groups by the acidification of the endosome, the electrostatic repulsions between cationic charges triggered polymer expansion (umbrella effect) and led to the liberation of siRNA into cytoplasm.

To successfully complex siRNA, the ratios of components needed to be optimized. In this research, two types of ratios were taken into consideration including mass ratio and charge ratio. Mass ratio (MS) describes the ratio between the mass of the inorganic core and that of siRNA. MS was optimized in the previous study in our group and fixed at $MS = 10$ [28]. The charge ratio represented the molar ratio between the number of positive charges of polymers (those of amino groups) and that of negative charges of siRNA (phosphate groups). Herein, there were two charge ratios to optimize including PLR/siRNA (CR) and chitosan/siRNA (CS). The following parts aimed to optimize these ratios by evaluating their impacts on the siRNA protection capacity and the siRNA transfection efficiency.

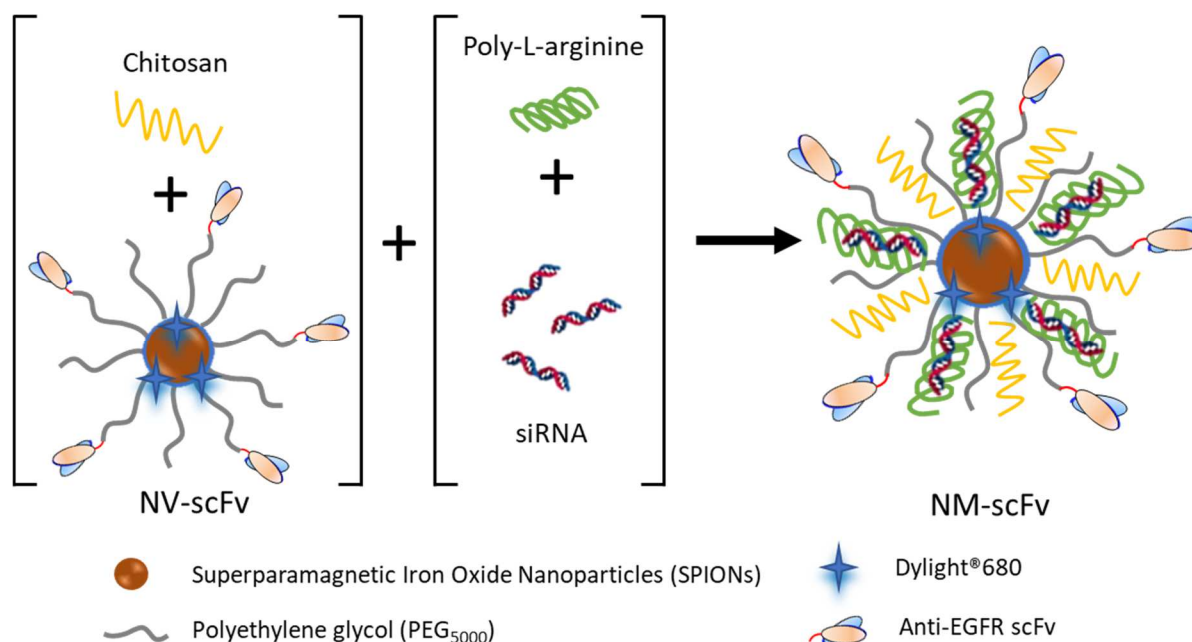


Fig. 4. Schematic representation of the targeted nanomedicine (NM-scFv) complexation between targeted nanovector (NV-scFv), siRNA and cationic polymers (Poly-L-arginine and Chitosan).

3.2.1 Optimization of transfection conditions

Before optimizing the charge ratios, relevant siRNA transfection conditions were required to clarify the difference between the tested formulations. According to the previous studies, the period between the treatment and the analysis was fixed at 72h to have enough time for the inhibition of the GFP protein (analysis time) [8,29]. Here, two parameters were studied to obtain an efficient transfection: i) the medium in which the transfection was performed (serum-free vs complete medium with 10% serum) and ii) the contact time between our NM-scFv with cells (4h vs 72h). The tested formulation (NM₀-scFv) was formulated using the following component ratios: MS=10; CR=4; and CS=30.

The NM₀-scFv was incubated with the cells either in Opti-MEM™ – a popular serum-free medium (-Serum) or in complete medium (+Serum). Two contact times, 4h or 72h were tested. For the short contact time, the NM₀-scFv was removed after 4h. For the contact time of 72h, the NM₀-scFv remained in contact with cells until the analysis. The cells in Opti-MEM™ were supplemented with serum after 4h to obtain a final concentration of 10%. This supplementation in serum helped to preserve cells from cell-death in serum-free medium.

The results (Fig. 5) showed that the transfection made in Opti-MEM™ was more efficient than in normal culture medium: 42.0±1.8% vs 28.1±0.9% for 4h and 50.1±0.7% vs 33.9±2.1% for 72h of incubation time. On the other hand, the contact time between NM₀-scFv and cells played also a relevant role. In the same condition of transfection (-Serum or +Serum), the transfection efficiency was better for the contact time of 72h compared to the short contact time of 4h (50.1±0.7% vs 42.0±1.8% for -Serum and 33.9±2.1% vs 28.1±0.9% for +Serum).

Taking into account these results, all the subsequent transfections in this study were performed in serum-free medium (Opti-MEM™) for 4h and the NM-scFv was kept in contact with the cells in normal medium for additional 68h until the analysis.

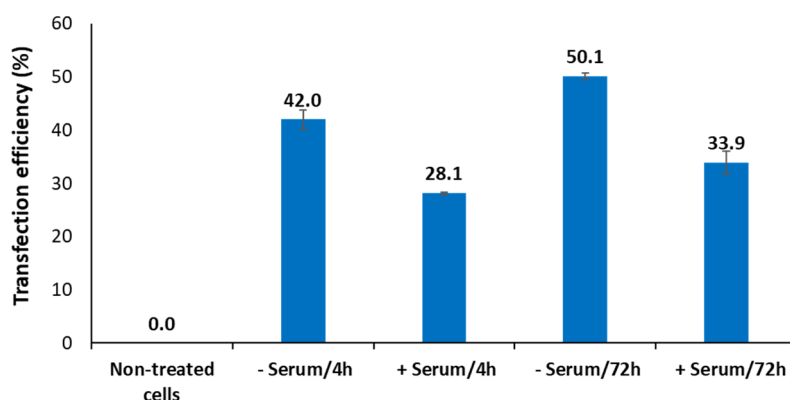


Fig. 5. Transfection efficiency of the NM₀-scFv at different conditions of transfection: with (+) or without (-) serum and at different contact times: 4h or 72h with MDA-MB-231 cells.

3.2.2 Optimization of the formulation parameters for an efficient siRNA transfection

The next step was to optimize the charge ratios including CR and CS. Both CR and CS were shown to be important for an efficient siRNA transfection [8,19,28]. A design of experiments was used to optimize these ratios. To construct this design of experiments, it was necessary to determine the levels of each ratio in our design.

In the case of CR, as PLR played a major role in siRNA complexation, the levels of CR had to be optimized to obtain a maximal siRNA protection capacity [8]. In this experiment, siRNA was complexed with PLR at different CR values from 0 to 10 and subsequently added to NV2-scFv. siRNA retention was evaluated using agarose gel electrophoresis. After the electrophoresis, free siRNA migrated and appeared as fluorescent bands, whereas protected siRNA remained in the loading wells. Without heparin addition, no fluorescent band was observed for formulations prepared with $CR \geq 2$, and with heparin addition, the fluorescent band of released siRNA from the formulations was detected (Fig. 6A). This result indicated that $CR \geq 2$ was required to obtain a complete siRNA complexation.

Nevertheless, as a strong cationic polymer, poly-L-arginine is susceptible to cause a cytotoxicity. To ensure the safety of our NM-scFv for further applications, a MTT cytotoxicity test was performed on MDA-MB-231 cells. In this experiment, the formulations of siRNA, PLR, and NV2-scFv at different CR were incubated with cancer cells for 72h. Non-treated cells and cells treated with H₂O₂ were used as controls. Cytotoxicity was observed for formulations with $CR \geq 20$ compared to non-treated cells and no cytotoxicity was recorded for formulations with $CR \leq 10$ (Fig. 6B). The levels of CR in our design of experiments were thus chosen between 2 and 10.

Concerning CS, the research of Bruniaux et al. showed that GFP down-regulation efficiency of non-targeted nanomedicine increased following CS up to its maximum at CS=30 and then decreased. The levels of CS in this study were varied from 10 to 50 to provide a maximal design space [8].

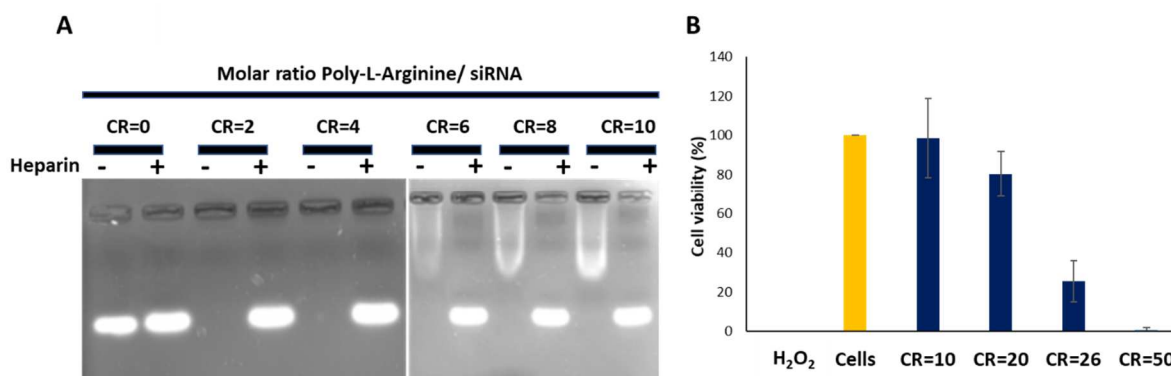


Fig. 6. Optimization of the PLR/siRNA charge ratio (CR). A: Gel retardation assay to detect free siRNA in formulations of siRNA, poly-L-arginine and NV2-scFv at different CR with (+) or without (-) heparin. B: Cellular viability of MDA-MB-231 cells treated with different formulations of siRNA, poly-L-arginine and NV2-scFv at different CR.

Based on these results, a full factorial design of experiments was created with the levels varied from 2 to 10 for CR and from 10 to 50 for CS. Three center points were included in the model and one response, the transfection efficiency, was analyzed (Table SI 2). The tested nanomedicine was made of NV₂-scFv to deliver a model siRNA (anti-GFP siRNA) into MDA-MB-231/GFP+ cells. All tested NM-scFv were controlled in terms of size (Table SI 2). Cells were analyzed using flow cytometry to measure the fluorescence intensity of GFP. Successful transfection of anti-GFP siRNA resulted in reduced GFP fluorescence compared to non-treated cells that was presented by two populations of cells following the GFP fluorescence intensity (Fig. 7A). The transfection efficiency was calculated based on the percentage of the cells with reduced GFP fluorescence intensity over the analyzed cells (Fig. 7B).

The regression analysis of the model indicated a R^2 of 99.76% with a predicted R^2 of 99.45% and an adjusted R^2 of 99.66%. These values, as well as a non-significant lack of fit ($p=0.226$), indicated a good fitting of the model, permitting further interpretation of the data. Together with the normalized effects chart (Fig. 7C), CR was remarked to have the most significant impact on the transfection efficiency ($p<0.001$). The transfection efficiency increased from $13.9\pm1.1\%$ to $69.4\pm0.5\%$ while CR varied from 2 to 10. On the other hand, a significant impact but less than that of CR (Table SI 3) on transfection efficiency was recorded for CS ($p=0.01$). The transfection efficiency increased when CS decreased (effect <0). The interaction between CS and CR displayed also a significant impact on transfection efficiency ($p<0.001$). This impact was less important than that of CR alone but more important than CS alone (Table SI 3). When CR was low (CR=2), the transfection efficiency increased with the increase of CS ($13.9\pm1.1\%$ for CS=10 vs $21.7\pm1.2\%$ for CS=50). On the contrary, when CR was high (CS=10), the transfection efficiency decreased following the increase of CS ($69.4\pm0.5\%$ for CS=10 vs $56.9\pm1.9\%$ for CS=50). These results indicated that there was an additive effect between chitosan and PLR and an equilibrium of both polymers was necessary for a good transfection efficiency. In summary, a high PLR amount and a low amount of chitosan were more favorable to high transfection efficiency.

Finally, the optimal ratios were determined using the optimization function of Minitab. To obtain a maximal transfection efficiency, the optimal CR and CS should be both fixed at 10. With these parameters, the predicted transfection efficiency was $69.4 \pm 0.5\%$. This value corresponded to the value obtained in the performed experiments. Comparison of this result with the size distribution of the different formulations (between $100.0 \pm 0.5\text{nm}$ and $193.4 \pm 5.4\text{nm}$) suggested a correlation between the maximal transfection efficiency and the lowest size (Table SI 2). In the literature, a similar phenomenon has been observed in the study of Huang et al. for the internalization of gold nanoparticles [30]. Concerning the charge ratios, our CR was higher than that in the study of Ben Djemaa et al. (CR=2) but similar to the study of Zhao et al. for siRNA delivery [2,31]. Nevertheless, the transfection efficiency was similar in three mentioned studies (around 70%). These experiments demonstrated not only the perspective of our NM-scFv as a siRNA delivery system but also the major effect of charge ratios and the size on the final gene silencing efficiency.

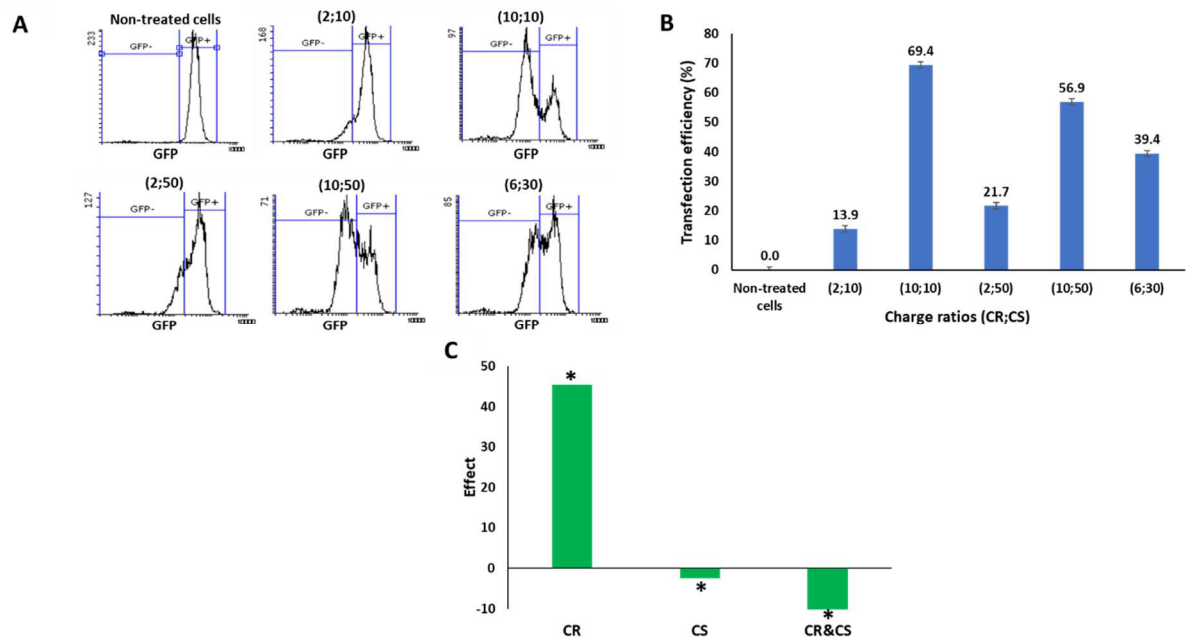


Fig. 7. Anti-GFP siRNA transfection efficiency. A: MDA-MB231 population following the GFP signal after transfection. B: Mean transfection efficiency of NM-scFv made of NV2-scFv with different molar ratios of Poly-L-Arginine/ siRNA (CR) and Chitosan/ siRNA (CS). C: Normalized effects chart for the main factors (CS or CR) and two-factor interaction (CR&CS) on transfection efficiency. Asterisk (*) indicates statistically significant factors with $p < 0.05$.

3.3 Efficiency of the optimized targeted nanomedicine

3.3.1 *In vitro* stealthiness

As shown in 3.1.1, the enhancement in PEG density improved the anti-EGFR scFv conjugation onto NV and resulted in a better functionality for our NV-scFv. However, the initial purpose was to improve the NM-scFv stealthiness that remained in question. Activation of the complement experiment (CH50

test) was performed to evaluate the impact of i) anti-EGFR scFv conjugation and ii) improvement in PEG density on the NM stealthiness.

As the stealthiness of NM is also dependent on the physicochemical properties [26], all the nanomedicines' physicochemical properties were controlled (Table II). There was an increase in the size of nanomedicines compared to nanovectors (97.4 ± 0.7 nm for NM1 vs 76.6 ± 5.3 nm for NV1) and the charge was lightly positive due to the presence of exceeded cationic polymers ($+4.5 \pm 3.5$ mV for NM1 vs -2.8 ± 2.4 mV for NV1). Nevertheless, the size around 100 nm with a narrow size distribution ($PDI < 0.3$) remained interesting for siRNA nanomedicines associated by electrostatic interactions.

Furthermore, the increase in PEG density might result in less condensed packaging of siRNA with cationic polymers. It was correlated to an increase in the size of NM2 and NM2-scFv compared to NM1 and NM1-scFv (109.6 ± 4.5 and 100.0 ± 2.3 nm vs 97.4 ± 0.7 and 92.2 ± 1.3 nm) [32,33].

Table II. Physicochemical properties of the evaluated nanomedicines.

	NM1	NM1-scFv	NM2	NM2-scFv
D_H (nm) (in intensity)	97.4 ± 0.7	92.2 ± 1.3	109.6 ± 4.5	100.0 ± 2.3
PDI	0.27 ± 0.02	0.23 ± 0.01	0.27 ± 0.01	0.25 ± 0.02
ζ (mV, pH 7.4)	$+4.5 \pm 3.5$	$+6.7 \pm 1.2$	$+5.4 \pm 1.3$	$+9.2 \pm 0.7$

Complement consumption was evaluated as the lytic capacity of the serum toward 50% of antibody-sensitized sheep erythrocytes (CH50 units) after exposure to the evaluated nanomedicines (Fig. 8). For the same type of NM and the same PEG density, the NM-scFv adsorbed a larger amount of serum proteins than the nanomedicine without scFv (between 25 and 150 μ g of iron/mL of NHS, NM1-scFv consumed 20 to 40% of CH50 units vs 10 to 15% for NM1). This result showed that the presence of conjugated anti-EGFR scFv as predicted increased the absorption of protein onto the NM's surface and may consequently prevent the long-circulating properties of PEG [34].

Despite the bigger size that may lead to a decline in stealthiness [26], the increase in PEG density helped NM2-scFv and NM2 to reduce the adsorption of serum proteins onto the nanomedicine surface and improved their stealthiness. For the whole evaluated range of NM concentrations (from 0 to 250 μ g of iron/mL of NHS), CH50 unit consumption was more important for NM1-scFv and NM1 than that of NM2-scFv and NM2. Especially, in the zone of interest from 125 to 188 μ g of iron/mL of NHS, the CH50 unit consumption was dramatically increased from 30 to 100% for NM1-scFv while that of NM2-scFv varied from 10 to 50% and only reached 100% at 250 μ g of iron/mL of NHS.

Though the confirmation of NM's stealthiness *in vivo* is unavoidable, these results revealed that by increasing the PEG density, there was a great perspective to improve our NM-scFv stealthiness for the further *in vivo* application.

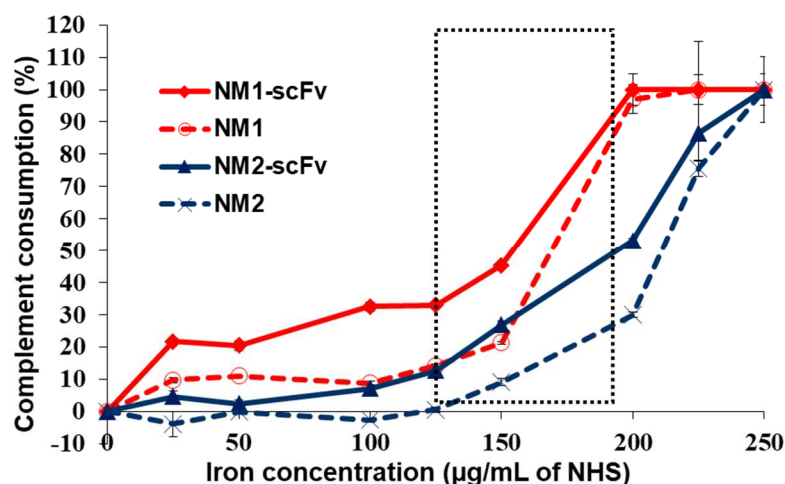


Fig. 8. Complement consumption by different NM according to iron concentration (μg of iron/mL of normal human serum). Dotted line zone presents the zone of interest concentrations for *in vivo* injection (125-188 μg of iron/mL of NHS).

3.3.2 Cellular internalization

To confirm the active targeting properties of NM-scFv, a cellular internalization experiment was performed with the optimal NM-scFv into MDA-MB-231 cells. The NM-scFv was prepared with control siRNA at the optimal ratios of MS=10; CR=10; and CS=10. The fluorescence signal of DylightTM680 was followed and compared. If the NMs internalize into the cancer cells, DylightTM680 fluorescence signal will be detected. Otherwise, there is no fluorescence detected for non-treated cells (Fig. 9A).

As shown in Fig. 9B, the DylightTM680 fluorescence intensity of internalized NM-scFv was higher than the non-targeted NM by a factor of 1.5 ($p < 0.01$). This increase in fluorescence intensity demonstrated a better cellular internalization of targeted NM compared to non-targeted NM. This better internalization could be explained by the increased uptake via receptor-mediated endocytosis due to anti-EGFR scFv. In comparison with the NV-scFv, the NM-scFv internalized better into the MDA-MB-231 cells. This phenomenon could be explained by the charge of the nanoparticles. The positively charged nanoparticles were more favorable in internalization than negatively charged nanoparticles due to the interaction between positive charges of nanoparticles and negatively charged cell membrane [30].

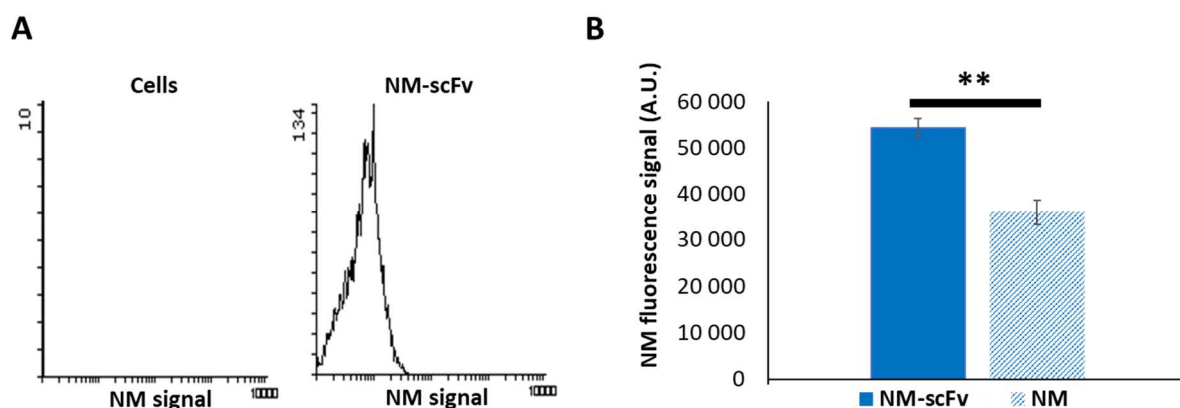


Fig. 9. Internalization of NMs into MDA-MB-231 cells by following Dylight™680 fluorescence signal. A) Fluorescence profiles obtained with flow cytometer of cells treated (right figure) or not (left figure) with NM-scFv. B) Fluorescence signal of internalized NM-scFv and NM. Double asterisk (**) indicates statistically significant factors with $p < 0.01$.

3.3.3 Transfection efficiency

With the optimal ratios at CR=10 and CS=10, our targeted nanomedicine was compared to the non-targeted NM and two other commercialized transfection agents: Oligofectamine® and Lipofectamine® in terms of transfection efficiency. Oligofectamine® and Lipofectamine® are two liposomal agents commonly used for *in vitro* siRNA transfection. The cationic lipids in the lipid bilayer structure can interact with the negative siRNA to form an ionic complex to immobilize and deliver siRNA across the cell membrane [35,36].

The tested formulations were firstly re-controlled in terms of physicochemical characteristics with DLS and TEM analysis. On the one hand, the size of NM and NM-scFv evaluated with DLS was found to be suitable for IV injection, which was inferior to 200nm with a narrow size distribution (Table SI 1). On the other hand, the TEM analysis revealed that the state of SPIONs in different steps of synthesis or formulation remained unchanged and not impacted by the other components. This observation may confirm its stability and its integrity in the formulation with siRNA (Table SI 1; Fig. SI 1). As expected, the size of SPION evaluated with TEM was smaller than that measured with DLS. The presence of hydration layer around SPIONs' core can explain this difference when the sample was observed in the solvated state with DLS. On the contrary, the TEM analysis allowed us to observe the SPION core in the dry state.

In the next step, the siRNA protection capacity of the final formulation was evaluated on agarose gel by electrophoresis method. Without added heparin, no fluorescent band was observed for the complexed siRNA. On the contrary, with added heparin, the fluorescent band of complexed siRNA was found with the same intensity as naked siRNA's (Fig. 10A). This experiment confirmed that siRNA was completely complexed and protected.

In Fig. 10B, the transfection efficiency of the targeted nanomedicine was higher than that of the non-targeted NM by a factor of 3.0 ($69.4 \pm 0.5\%$ vs $25.3 \pm 0.2\%$). This result demonstrated a targeted siRNA

delivery into TNBC cells of our NM-scFv. This targeting delivery could be explained by i) the specific interaction between the conjugated anti-EGFR scFv and EGFR receptors overexpressed on MDA-MB-231 cells that resulted in a better cellular internalization [34] and ii) the successful endosomal escape of siRNA with the help of polymers. The transfection efficiency of Oligofectamine® and Lipofectamine® in the same conditions was $55.3 \pm 3.9\%$ and $97.0 \pm 1.2\%$ respectively. Though Lipofectamine® displayed a better transfection efficiency than our NM-scFv, these cationic lipids may cause a susceptible toxicity due to their ability to disrupt the cellular and mitochondrial membrane. Moreover, these commercial transfection agents are not suitable for *in vivo* application [35,36]. Thus, an efficient alternative for siRNA delivery can be achieved both *in vitro* and *in vivo* with our NM-scFv.

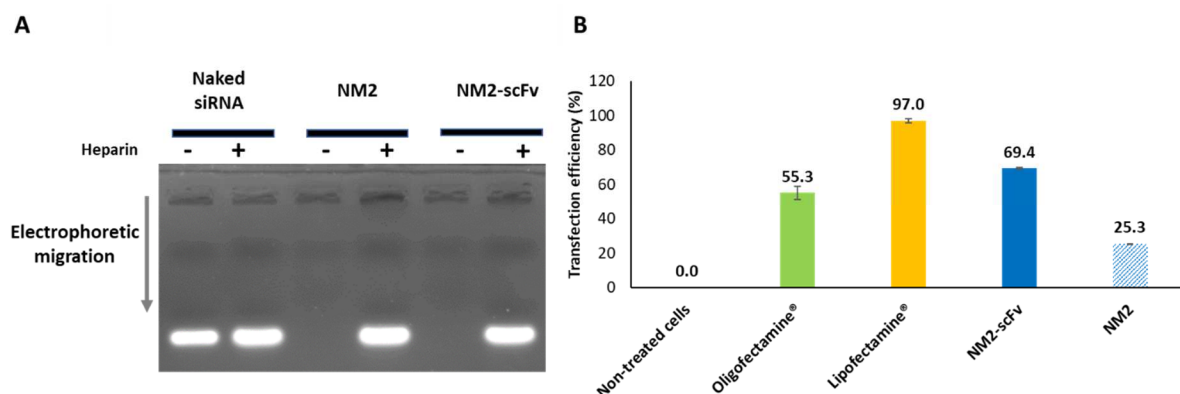


Fig. 10. Targeted nanomedicine compared to non-targeted nanomedicine and commercialized transfection agents. A: Gel retardation assay to detect free siRNA in nanomedicines with (+) or without (-) heparin. B: Anti-GFP siRNA transfection efficiency of optimized targeted nanomedicine (NM2-scFv) compared to non-targeted nanomedicines, Oligofectamine®, and Lipofectamine®.

4 Conclusion

In this study, a targeted nanomedicine for siRNA delivery into triple negative breast cancer cells was developed and optimized. This targeted nanomedicine (NM-scFv) was based on the targeted nanovector (NV-scFv) functionalized with a humanized anti-EGFR scFv antibody fragment as targeting ligand and subsequently associated with siRNA, chitosan, and PLR.

The NV-scFv was firstly optimized in terms of PEG layer density. By changing the PEG/iron molar ratio from 0.3 to 0.6, an increase by a factor of 3.7 in PEG layer density was achieved for our optimized NV-scFv (873 ± 4 vs 236 ± 3 of PEGs/NV-scFv). This increase showed an important impact on: i) the number of conjugated active targeting ligands (13 vs 9 of scFv/NV-scFv) resulting in an increase in cellular internalization by a factor of 2 for 24h of incubation time and ii) the improvement in stealthiness of the final NM-scFv confirmed by CH50 test. In fact, in the zone of interest for *in vivo* injection (125-188µg of iron/mL of NHS), there was a significant decrease in protein adsorption for our final NM-scFv (10-50% vs 30-100% of CH50 unit consumption).

In the second step, the formulation between NV-scFv and siRNA was performed with the addition of chitosan and poly-L-arginine and optimized in terms of the ratios of components. Two necessary ratios for the formulation were evaluated including: i) Chitosan/siRNA charge ratio (CS) and ii) PLR/siRNA

652 charge ratio (CR). The optimal parameters for our NM-scFv were determined at CS=10 and CR=10.
653 Among these parameters, CR was shown to play the most important role on the transfection efficiency
654 with a positive effect. CS and the interaction CR&CS presented also a significant impact with a
655 negative effect but less important than that of CR. The optimized NM-scFv presented suitable
656 physicochemical properties for IV injection with a size of $100.0 \pm 2.3 \text{ nm}$, a narrow size distribution
657 ($\text{PDI} = 0.25 \pm 0.02$) and an almost neutral surface charge ($+9.2 \pm 0.7 \text{ mV}$). Moreover, the benefit of the
658 active targeting with the anti-EGFR scFv was confirmed with a higher cellular internalization into MDA-
659 MB-231 by a factor of 1.5. Finally, NM-scFv exhibited an efficient siRNA protection capacity that was
660 confirmed with a gel electrophoresis experiment and a promising *in vitro* transfection efficiency
661 ($69.4 \pm 0.5\%$) into TNBC cancer cells with anti-GFP siRNA.

662 All the results demonstrated the promising application of our targeted nanomedicine functionalized
663 with humanized anti-EGFR antibody fragment for efficient targeted siRNA delivery into TNBC tumors.

Acknowledgments

The authors would like to thank Laurie Lajoie, Valérie Gouilleux and Christine Dhommee from *Plateforme Scientifique et Technique, Analyse des systèmes biologiques département des cytométries, University of Tours* for their help in the experiments with flow cytometry. We are grateful to Pierre-Ivan Raynal (Département des Microscopies, Université de Tours, France). Our data were obtained with the assistance of the IBiSA Electron Microscopy Facility of the University of Tours. This work was supported by the 'Canceropole Grand Ouest' and especially by the Emergence CGO 2019 NANOTIF project. This work was supported by the French National Research Agency under the program "Investissements d'avenir" Grant Agreement LabEx MAblmprove (ANR-10-LABX-53-01).

Conflict of interest

The authors declare that they have no conflict of interest.

675 References

- 676 [1] A. Lee, M.B.A. Djamgoz, Triple negative breast cancer: Emerging therapeutic modalities and
677 novel combination therapies, *Cancer Treat. Rev.* 62 (2018) 110–122.
678 <https://doi.org/10.1016/j.ctrv.2017.11.003>.
- 679 [2] S. Ben Djemaa, S. David, K. Hervé-Aubert, A. Falanga, S. Galdiero, E. Allard-Vannier, I.
680 Chourpa, E. Munnier, Formulation and in vitro evaluation of a siRNA delivery nanosystem
681 decorated with gH625 peptide for triple negative breast cancer theranosis, *Eur. J. Pharm.*
682 *Biopharm. Off. J. Arbeitsgemeinschaft Pharm. Verfahrenstechnik EV.* 131 (2018) 99–108.
683 <https://doi.org/10.1016/j.ejpb.2018.07.024>.
- 684 [3] K.A. Akshata Desai, Triple Negative Breast Cancer – An Overview, *Hered. Genet.* (2012).
685 <https://doi.org/10.4172/2161-1041.S2-001>.
- 686 [4] S. Hurvitz, M. Mead, Triple-negative breast cancer: advancements in characterization and
687 treatment approach, *Curr. Opin. Obstet. Gynecol.* 28 (2016) 59–69.
688 <https://doi.org/10.1097/GCO.0000000000000239>.
- 689 [5] Y.-K. Oh, T.G. Park, siRNA delivery systems for cancer treatment, *Adv. Drug Deliv. Rev.* 61
690 (2009) 850–862. <https://doi.org/10.1016/j.addr.2009.04.018>.
- 691 [6] S. Ben Djemaa, E. Munnier, I. Chourpa, E. Allard-Vannier, S. David, Versatile electrostatically
692 assembled polymeric siRNA nanovectors: Can they overcome the limits of siRNA tumor
693 delivery?, *Int. J. Pharm.* 567 (2019) 118432. <https://doi.org/10.1016/j.ijpharm.2019.06.023>.
- 694 [7] C. Xu, J. Wang, Delivery systems for siRNA drug development in cancer therapy, *Asian J.*
695 *Pharm. Sci.* 10 (2015) 1–12. <https://doi.org/10.1016/j.ajps.2014.08.011>.
- 696 [8] J. Bruniaux, S.B. Djemaa, K. Hervé-Aubert, H. Marchais, I. Chourpa, S. David, Stealth magnetic
697 nanocarriers of siRNA as platform for breast cancer theranostics, *Int. J. Pharm.* 532 (2017) 660–
698 668. <https://doi.org/10.1016/j.ijpharm.2017.05.022>.
- 699 [9] C. Alric, K. Hervé-Aubert, N. Aubrey, S. Melouk, L. Lajoie, W. Mème, S. Mème, Y.
700 Courbebaisse, A.A. Ignatova, A.V. Feofanov, I. Chourpa, E. Allard-Vannier, Targeting HER2-
701 breast tumors with scFv-decorated bimodal nanoprobe, *J. Nanobiotechnology.* 16 (2018) 18.
702 <https://doi.org/10.1186/s12951-018-0341-6>.
- 703 [10] V. Venugopal, S. Krishnan, V.R. Palanimuthu, S. Sankarankutty, J.K. Kalaimani, S. Karupiah,
704 N.S. Kit, T.T. Hock, Anti-EGFR anchored paclitaxel loaded PLGA nanoparticles for the treatment
705 of triple negative breast cancer. In-vitro and in-vivo anticancer activities, *PLOS ONE.* 13 (2018)
706 e0206109. <https://doi.org/10.1371/journal.pone.0206109>.
- 707 [11] J. Pi, J. Jiang, H. Cai, F. Yang, H. Jin, P. Yang, J. Cai, Z.W. Chen, GE11 peptide conjugated
708 selenium nanoparticles for EGFR targeted oridonin delivery to achieve enhanced anticancer
709 efficacy by inhibiting EGFR-mediated PI3K/AKT and Ras/Raf/MEK/ERK pathways, *Drug Deliv.*
710 24 (2017) 1549–1564. <https://doi.org/10.1080/10717544.2017.1386729>.
- 711 [12] M.W. Kim, H.Y. Jeong, S.J. Kang, I.H. Jeong, M.J. Choi, Y.M. You, C.S. Im, I.H. Song, T.S. Lee,
712 J.S. Lee, A. Lee, Y.S. Park, Anti-EGF Receptor Aptamer-Guided Co-Delivery of Anti-Cancer
713 siRNAs and Quantum Dots for Theranostics of Triple-Negative Breast Cancer, *Theranostics.* 9
714 (2019) 837–852. <https://doi.org/10.7150/thno.30228>.
- 715 [13] C. Alric, N. Aubrey, É. Allard-Vannier, A. di Tommaso, T. Blondy, I. Dimier-Poisson, I. Chourpa,
716 K. Hervé-Aubert, Covalent conjugation of cysteine-engineered scFv to PEGylated magnetic
717 nanoprobe for immunotargeting of breast cancer cells, *RSC Adv.* 6 (2016) 37099–37109.
718 <https://doi.org/10.1039/C6RA06076E>.
- 719 [14] Ida Genta, Enrica Chiesa, Barbara Colzani, Tiziana Modena, Bice Conti, Rossella Dorati, GE11
720 Peptide as an Active Targeting Agent in Antitumor Therapy: A Minireview, *Pharmaceutics.* 10
721 (2017) 2. <https://doi.org/10.3390/pharmaceutics10010002>.
- 722 [15] A.V. Lakhin, V.Z. Tarantul, L.V. Gening, Aptamers: problems, solutions and prospects, *Acta*
723 *Naturae.* 5 (2013) 34–43.
- 724 [16] A. Pawar, P. Prabhu, Nanosoldiers: A promising strategy to combat triple negative breast
725 cancer, *Biomed. Pharmacother.* 110 (2019) 319–341.
726 <https://doi.org/10.1016/j.biopha.2018.11.122>.
- 727 [17] M. Zhang, H.S. Kim, T. Jin, J. Woo, Y.J. Piao, W.K. Moon, Near-infrared photothermal therapy
728 using anti-EGFR-gold nanorod conjugates for triple negative breast cancer, *Oncotarget.* 8
729 (2017). <https://doi.org/10.18632/oncotarget.21243>.
- 730 [18] Z. Lakhri, M. Pugnère, C. Henriquet, A. di Tommaso, I. Dimier-Poisson, P. Billiald, M.O. Juste,
731 N. Aubrey, A method to confer Protein L binding ability to any antibody fragment, *MAbs.* 8 (2016)
732 379–388. <https://doi.org/10.1080/19420862.2015.1116657>.

- [19] S. David, H. Marchais, D. Bedin, I. Chourpa, Modelling the response surface to predict the hydrodynamic diameters of theranostic magnetic siRNA nanovectors, *Int. J. Pharm.* 478 (2015) 409–415. <https://doi.org/10.1016/j.ijpharm.2014.11.061>.
- [20] Z. Jia, C. Tian, Quantitative determination of polyethylene glycol with modified Dragendorff reagent method, *Desalination*. 247 (2009) 423–429. <https://doi.org/10.1016/j.desal.2008.09.004>.
- [21] M.M. Bradford, A rapid and sensitive method for the quantitation of microgram quantities of protein utilizing the principle of protein-dye binding, *Anal. Biochem.* 72 (1976) 248–254. [https://doi.org/10.1016/0003-2697\(76\)90527-3](https://doi.org/10.1016/0003-2697(76)90527-3).
- [22] E. Allard-Vannier, S. Cohen-Jonathan, J. Gautier, K. Hervé-Aubert, E. Munnier, M. Soucé, P. Legras, C. Passirani, I. Chourpa, Pegylated magnetic nanocarriers for doxorubicin delivery: A quantitative determination of stealthiness in vitro and in vivo, *Eur. J. Pharm. Biopharm.* 81 (2012) 498–505. <https://doi.org/10.1016/j.ejpb.2012.04.002>.
- [23] E. Blanco, H. Shen, M. Ferrari, Principles of nanoparticle design for overcoming biological barriers to drug delivery, *Nat. Biotechnol.* 33 (2015) 941–951. <https://doi.org/10.1038/nbt.3330>.
- [24] K. Hervé, L. Douziech-Eyrolles, E. Munnier, S. Cohen-Jonathan, M. Soucé, H. Marchais, P. Limelette, F. Warmont, M.L. Saboungi, P. Dubois, I. Chourpa, The development of stable aqueous suspensions of PEGylated SPIONs for biomedical applications, *Nanotechnology*. 19 (2008) 465608. <https://doi.org/10.1088/0957-4484/19/46/465608>.
- [25] J.L. Perry, K.G. Reuter, M.P. Kai, K.P. Herlihy, S.W. Jones, J.C. Luft, M. Napier, J.E. Bear, J.M. DeSimone, PEGylated PRINT Nanoparticles: The Impact of PEG Density on Protein Binding, Macrophage Association, Biodistribution, and Pharmacokinetics, *Nano Lett.* 12 (2012) 5304–5310. <https://doi.org/10.1021/nl302638g>.
- [26] J.S. Suk, Q. Xu, N. Kim, J. Hanes, L.M. Ensign, PEGylation as a strategy for improving nanoparticle-based drug and gene delivery, *Adv. Drug Deliv. Rev.* 99 (2016) 28–51. <https://doi.org/10.1016/j.addr.2015.09.012>.
- [27] Q. Yang, S.W. Jones, C.L. Parker, W.C. Zamboni, J.E. Bear, S.K. Lai, Evading Immune Cell Uptake and Clearance Requires PEG Grafting at Densities Substantially Exceeding the Minimum for Brush Conformation, *Mol. Pharm.* 11 (2014) 1250–1258. <https://doi.org/10.1021/mp400703d>.
- [28] S. David, H. Marchais, K. Hervé-Aubert, D. Bedin, A.-S. Garin, C. Hoinard, I. Chourpa, Use of experimental design methodology for the development of new magnetic siRNA nanovectors (MSN), *Int. J. Pharm.* 454 (2013) 660–667. <https://doi.org/10.1016/j.ijpharm.2013.05.051>.
- [29] S. Ben Djemaa, K. Hervé-Aubert, L. Lajoie, A. Falanga, S. Galdiero, S. Nedellec, M. Soucé, E. Munnier, I. Chourpa, S. David, E. Allard-Vannier, gH625 Cell-Penetrating Peptide Promotes the Endosomal Escape of Nanovectorized siRNA in a Triple-Negative Breast Cancer Cell Line, *Biomacromolecules*. 20 (2019) 3076–3086. <https://doi.org/10.1021/acs.biomac.9b00637>.
- [30] N. Huang, H. Li, Q. Jin, J. Ji, Surface and Size Effects on Cell Interaction of Gold Nanoparticles with Both Phagocytic and Nonphagocytic Cells, *Langmuir*. 29 (2013) 9138–9148. <https://doi.org/10.1021/la401556k>.
- [31] Z.-X. Zhao, S.-Y. Gao, J.-C. Wang, C.-J. Chen, E.-Y. Zhao, W.-J. Hou, Q. Feng, L.-Y. Gao, X.-Y. Liu, L.-R. Zhang, Q. Zhang, Self-assembly nanomicelles based on cationic mPEG-PLA-b-Polyarginine(R15) triblock copolymer for siRNA delivery, *Biomaterials*. 33 (2012) 6793–6807. <https://doi.org/10.1016/j.biomaterials.2012.05.067>.
- [32] S. Mao, M. Neu, O. Germershaus, O. Merkel, J. Sitterberg, U. Bakowsky, T. Kissel, Influence of Polyethylene Glycol Chain Length on the Physicochemical and Biological Properties of Poly(ethylene imine)- graft -Poly(ethylene glycol) Block Copolymer/SiRNA Polyplexes, *Bioconjug. Chem.* 17 (2006) 1209–1218. <https://doi.org/10.1021/bc060129j>.
- [33] C. Yang, S. Gao, F. Dagnæs-Hansen, M. Jakobsen, J. Kjems, Impact of PEG Chain Length on the Physical Properties and Bioactivity of PEGylated Chitosan/siRNA Nanoparticles in Vitro and in Vivo, *ACS Appl. Mater. Interfaces*. 9 (2017) 12203–12216. <https://doi.org/10.1021/acsami.6b16556>.
- [34] N.T. Huynh, E. Roger, N. Lautram, J.-P. Benoît, C. Passirani, The rise and rise of stealth nanocarriers for cancer therapy: passive versus active targeting, *Nanomed.* 5 (2010) 1415–1433. <https://doi.org/10.2217/nnm.10.113>.
- [35] M. Braddock, *Nanomedicines: Design, Delivery and Detection*, Royal Society of Chemistry, 2016.
- [36] I. Kraja, R. Bing, N. Hiwatashi, B. Rousseau, D. Nalband, K. Kirshenbaum, R.C. Branski, Preliminary study of a novel transfection modality for in vivo siRNA delivery to vocal fold fibroblasts: Transfection Efficiency of Lipitoid Oligomers, *The Laryngoscope*. 127 (2017) E231–E237. <https://doi.org/10.1002/lary.26432>.